Published in final edited form as:

Nature. 2017 January 26; 541(7638): 554–557. doi:10.1038/nature21053.

Structural Basis of Co-translational Quality Control by ArfA and RF2 Binding to Ribosome

Fuxing Zeng[1], **Yanbo Chen**[1], **Jonathan Remis**[2], **Mrinal Shekhar**[3,4], **James C. Phillips**[4], **Emad Tajkhorshid**[1,3,4], and **Hong Jin**[1,3]

[1]Department of Biochemistry, University of Illinois at Urbana-Champaign

[2]Department of Molecular Biosciences, Northwestern University

[3]Center for Biophysics and Quantitative Biology, University of Illinois at Urbana-Champaign

[4]Beckman Institute for Advanced Science and Technology, University of Illinois at Urbana-Champaign

Abstract

Quality-control mechanisms intervene appropriately when defective translation events occur to preserve the intergrity of protein synthesis. Rescuing the ribosome translating on mRNAs absent of a stop codon is one of the co-translational quality control pathways in the cell. In many bacteria, ArfA recognizes stalled ribosome and recruits release factor RF2, which catalyzes the termination of protein synthesis [1–3]. While an induced-fit mechanism of ArfA/RF2-mediated nonstop mRNA surveillance has been reported [4], the molecular interaction between ArfA and RF2 in the ribosome that is responsible for the mechanism is unknown. Here we report a cryoEM structure of ArfA and RF2 in complex with the 70S ribosome that is bound to a nonstop mRNA. The structure, which is consistent with our kinetic and biochemical data, reveals the molecular interactions that enable ArfA to specifically recruit RF2, not RF1, into the ribosome and to promote RF2 to release the truncated protein product in this co-translational quality control pathway. The positively charged C-terminal domain of ArfA anchors in the mRNA entry channel of the ribosome. Further, binding of the ArfA and RF2 induces conformational changes in the ribosomal decoding center in a way that is similar to other protein-involved decoding processes. Specific interactions between residues in the N-terminal domain of ArfA and RF2 help RF2 attain a catalytically competent conformation for peptide release. Insights gained from this investigation provide a framework to understand recognition of the translational state of the ribosome by new proteins, and expand our knowledge of the decoding potential of the ribosome.

Correspondence to: Hong Jin.

Correspondence and requests for materials should be addressed to H.J.

The authors declare no competing financial interests.

Author contributions

F.Z. and H.J. designed the study. F.Z. purified ribosomes, proteins and tRNAs, processed EM data and built the atomic model. Y.C. did the mutagenesis and purified ArfA mutants. F.Z. and Y.C. performed the peptide release assay. F.Z., Y.C., H.J. and J.R. collected EM data. M.S., J.C.P. and E.T. provided computational support. F.Z., Y.C. and H.J. analyzed the data and refined the structure. F.Z. and Y.C. helped on manuscript preparation. H.J. wrote the paper. All authors discussed on the final manuscript.

Elegant surveillance mechanisms have evolved in the cell to ensure translation is error-free [5-7]. When a ribosome becomes involved in the translation of mRNAs that have no stop codons, an event called nonstop translation, it is destined to stall at the end of the mRNA, in a state unable to either elongate or terminate the nascent peptide chain, because its aminoacyl (A) site is unoccupied. Bacteria are known to have three mechanisms for resolving stalled ribosomal complexes that result from nonstop translation, all of which start with recognition of truncated mRNAs, and end with release of nascent polypeptides from the stalled ribosome [6, 7].

One of these mechanisms, the ArfA/RF2-mediated surveillance pathway, involves protein ArfA [1–3] and one of the class I protein release factors, RF2, that catalyzes peptide release during normal translational termination [8] and quality control [9]. Intriguingly, although the GGQ motif [10–12] in RF2 is required for peptide release in the pathway, the tripeptide SPF motif [8] that is essential for the stop-codon recognition by RF2, appears to be dispensable [2]. Furthermore, nucleotides in the 16S ribosomal RNA (rRNA) that are in the close vicinity of ArfA when it binds to the ribosome have been identified [13].

Despite these exciting developments, the molecular interactions that enable ArfA to recruit RF2 and help it adopt its catalytically competent conformation remain unknown. We previously demonstrated that peptide release catalyzed by ArfA and RF2 on a nonstop mRNA in the ribosome is achieved by an induced-fit mechanism [4], as seen in the tRNA decoding on a sense codon [14] and canonical termination on a stop codon [15]. Here we report the molecular interactions responsible for the mechanism revealed by electron cryo-microscopy (cryoEM) structure of the bacterial 70S ribosome bound to biologically-related RF2 with its GGQ motif methylated [4] and ArfA [16,17] proteins, reconstructed to an overall resolution of 3.52 Å (Fig. 1, Extended Data Figs 1 and 2, Extended data Table 1). The functional importance of these molecular interactions is further supported by results from our real-time kinetic experiments (Extended Data Table 2).

As expected [4], the ribosome is in a non-rotated conformation (Fig. 1a and 1b), and the 30S subunit is in a “closed” conformation [18]. The overall conformation of RF2 in the ribosome is similar to what reported on canonical termination complexes for stop-codon recognition [19–22] (Extended Data Fig. 3). ArfA adopts an extended conformation and interacts across the subunit interface of the ribosome reaching from the mRNA entry channel, across the decoding center, to the “B2a bridge”, the subunit junction that is formed by the helix 69 of the 23S rRNA (H69) and helix 44 of the 16S rRNA (h44) in the ribosome (Fig. 1c).

The positively-charged C-terminal region of ArfA (residue 33–44) inserts into the mRNA entry channel downstream of the A-site. Its highly conserved R41 and an upstream KGKG motif (residue 34–37, Extended Data Fig. 4a) interact with the phosphate backbone of the 16S rRNA that form the mRNA entry channel (Fig. 2a, Extended Data Figs. 5a and 5b), anchoring the protein in the subunit interface of the ribosome. Although the length and amino acid sequence of the C-terminal tail of ArfA vary with species, they all contain positively charged amino acids (Extended Data Fig. 4b). Furthermore, similar interactions were reported in the other two nonstop ribosomal complexes [23, 24]. Together, these

observations suggest that the proteins that are recruited to the ribosome stalled on a truncated mRNA recognize an empty ribosomal mRNA entry channel mainly via electrostatic interactions.

ArfA detects the presence of an empty A-site in the ribosome. Residues P23-E30 of ArfA interact with the ribosomal decoding center (Fig. 2b, Extended Data Fig. 5c). Conformational flexibility conferred by the loop 3 of ArfA (Extended Data Fig. 4a) and the 3′-end of the truncated mRNA in this region likely allows ArfA to accommodate one to two codons in the mRNA downstream from the ribosomal P-site (Extended Data Fig. 5d), in agreement with the results from biochemical experiments [14,13]. Binding of ArfA and RF2 to the ribosome induces conformational changes in the decoding center. One of the two bases essential for the decoding in h44, A1492 and A1493, stacks on A1913 of H69 in the 23S rRNA, a feature of the ribosomal decoding center that has been seen repeatedly when proteins "decode" the state of the A-site in the ribosome [22–26]. A1492 is modeled to stacks with A1913, and the base of A1493 appears to be disordered and is refined to a conformation that is flipped out of h44. A proline residue (P23) of ArfA stacks on A1492 (Fig. 2b). A P23A mutation decreases the k_{cat} of the peptide release reaction by about half (Fig. 2c, Extended Data Fig. 6a), suggesting the functional importance of the interaction between this proline and rRNA, which likely stabilizes the A-A stacking and helps establish a connection between the mRNA entry channel and the conformational state of 23S rRNA in the large subunit of the ribosome.

By contrast, while E30 of ArfA stacks with G530 of h18 of the 16SrRNA, an E30A mutation shows little change in the value of k_{cat} of the release reaction (Fig. 2c). Furthermore, as seen in the C-terminal tail of ArfA, electrostatic interactions between ArfA and rRNA are observed in this region (Extended Data Fig. 5c). However, single amino acid mutations of conserved positively-charged residues in ArfA from R26 to R41 only marginally affects the kinetics of the peptide release reaction catalyzed by RF2 (Figs. 2c, Extended Data Figs. 6a, 6b and 6c), suggesting redundancy of the electrostatic interactions between the rRNA and the C-terminal domain of ArfA in the pathway.

Notably, the SPF tripeptide motif [8] in RF2 indeed "falls" into the decoding pocket, but it does not interact with ArfA nor with the three essential nucleotides in the 16S rRNA, which are more than 5Å away. This observation not only explains why the SPF motif is functionally dispensable, but also suggests that ArfA is responsible for detecting the presence of an empty A site in the nonstop-stalled ribosome.

Sequence-specific interactions between ArfA and RF2 explain why only RF2 is recruited. Residues 27, 28 and 29 in ArfA form a β sheet (β1) anti-parallel to β5 in the region from residues 214, 215 and 216 in domain II of RF2 (Fig. 2b). Extensive hydrophobic interactions are observed between residues in α2 to loop 2 regions of ArfA and the β4 and β5 in domain II of RF2. The hydrophobic side chains of L19, L20, L24 and F25 in ArfA form a unique hydrophobic surface which packs with V198 and F217 of RF2 on one side, and with W319 of RF2 on the other (Fig. 2d). W319 resides in the so-called "switch loop" [25] that is suggested to be important for the peptide release by protein release factors. It is likely that the packing of W319 with the hydrophobic surface of ArfA stabilizes the switch loop,

thereby facilitating the catalytic function of RF2 for the peptide release. In contrast, RF1 cannot form similar hydrophobic interactions with ArfA, because it does not contain amino acids with bulky hydrophobic side chains at the equivalent positions of 198, 217 and 319 (Extended Data Fig. 7). Thus, the differences in the sequence between the two release factors in this region explain why RF2, rather than RF1, is recruited into the ribosome by ArfA.

The N-terminal domain of ArfA forms a tight helix and turn conformation which is nicely sandwiched between the α7 helix in RF2 and the interface of the 23S and 16S rRNAs (Figs. 3a and 3b), and this region is important for stabilizing the catalytically-competent conformation of RF2 for the peptide release in the ribosome. Positively charged K8 interacts with phosphate backbone of C1914 in H69 (Fig. 3a). Contrary to the redundant electrostatic interactions observed in the C-terminal domain of ArfA, a K8A mutation severely compromises the peptide release activity in the ribosome (Fig. 3c and 3d). Furthermore, a highly conserved G9 introduces a sharp turn of the backbone in this region. The conformation of the loop is stabilized by extensive hydrophobic interactions between highly conserved residues I11, A15 and A18 (Fig. 3b). A disruption of the G9-introduced turn or of the hydrophobic interactions in the loop severely compromises the peptide release activity of RF2 (Fig 3c and 3d, Extended Data Fig. 6d). Notably, impacts on the kinetics of the release reaction are nearly the same for the ArfA mutants with a point I11N mutation and with an N-terminal 18 amino acid truncation.

An isoleucine residue at position of 16 in ArfA (I16) at the junction of the loop and the helix forms hydrophobic interactions with F221 in the β5 of RF2 (Fig. 3b). This hydrophobic interaction is likely to be important for inducing RF2 into a catalytically competent conformation, because RF2 from *Thermus thermophilus*, which contains a glutamic acid (E) at the equivalent position of 221 but otherwise the same amino acids at the positions of 198, 217 and 319, can bind to the ribosome (Extended Data Fig. 8a) but fails to catalyze the peptide release reaction (Extended Data Fig. 8b).

Taken together, these results suggest that the molecular interactions observed in the N-terminal domain of ArfA with RF2 are important for positioning RF2 in a catalytic-competent form, and docking the universally conserved GGQ motif into the PTC of the ribosome. The PTC of the ribosome is in a fully induced state [26, 27], priming for the release of the nascent peptide in the ribosome.

In conclusion, our combined structural and biochemical investigation demonstrates how a rescuing signal generated by proteins down in the mRNA entry channel is transmitted over ~80 Å to the PTC of the large ribosomal subunit where the elongation of a nascent peptide chain is terminated (Fig. 4). The observation that a small protein such as ArfA can be recruited to facilitate the function of a release factor in terminating protein synthesis in the ribosome suggests a new way of translation regulation that can be used in the development of antibacterial and antigrowth therapeutics that target the translating ribosome.

Methods

Preparation of *E. coli* ribosomes, tRNAs and initiation factors

70S ribosomes from *E. coli* MRE600 strain [28] were prepared as described [29]. ArfA, RF2 and $tRNA^{fMet}$ were cloned from *E. coli* K12 strain [30] and were purified [4]. *E. coli* IF1, IF2, and IF3 were overexpressed and purified [31]. The mRNA with the sequence 5′-GGC AAG GAG GUA AAA AUG-3′ (P-site is underlined) was purchased from Dharmacon (Amersham/GE Healthcare).

Purification of the two biologically-related proteins, ArfAΔ17C and RF2 with fully methylated GGQ^m motif

The expression of the full-length *E. coli* ArfA and ArfA-homologue proteins from other bacterial species is subject to regulation of RNases and tmRNA-SmpB activity. In the absence of the tmRNA-SmpB system, the C-termnial 17 amino acids truncated protein ArfAΔ17C is produced by RNase III in *E.coli*, and is used to recruit RF2 for rescuing the stalled ribosome [16, 17, 32]. Furthermore, the glutamine of the universally conserved GGQ motif [10,11] in RF2 is methylated (GGQ^m) [12]. This conserved post-translational modification stimulates the catalytic function of RF2 by 10-fold *in vitro*[4] and is functionally important *in vivo*. Thus, the two biologically-related proteins, ArfAΔ17C and RF2 with the GGQ^m motif are used in this study and are referred to as ArfA and RF2, respectively, for clarity. Point mutations in ArfA were generated by mutagenesis and mutant ArfA proteins were purified in the same way as wildtype ArfA [4].

Preparation of charged $tRNA^{fMet}$

E. coli methionine-tRNA synthetase (MetRS) and methionyl-tRNA formyltransferase (FMT) were purified [33]. Aminoacylation and formylation of the $tRNA^{fMet}$ were performed as described previously [434]. Briefly, 20 μM $tRNA^{fMet}$ was incubated with 0.6 mM L-methionine, 1 μM L-[^{35}S]-methionine (PerkinElmer), 0.6 mM 10-formyltetrahydrofolate, 12 μM MetRS, 12 μM FMT, 10 mM ATP, and 0.02 U/μL pyrophosphatase at 37°C for 40 min in a buffer containing 100 mM HEPES-KOH, pH 7.6, 20 mM KCl, 10 mM $MgCl_2$ and 1 mM DTT. Charged fMet-$tRNA^{fMet}$ was purified by phenol:chloroform extraction followed by ethanol precipitation and stored in 2 mM NaOAc, pH 5.2.

Peptide release assay

The k_{cat} and $K_{1/2}$ of peptide release were measured as described [4]. The release complex was first formed by incubating ribosome (2 μM), mRNA (6 μM), IF1, IF2, IF3 (3μM each), fMet-$tRNA^{fMet}$ (3 μM) and GTP (2 mM) at 37 °C for 30 min in the buffer containing 50 mM Tris, pH 7.4, 70 mM NH_4Cl, 30 mM KCl, 10 mM $MgCl_2$ and 5 mM β-mercaptoethanol. The complex was purified by sucrose cushion. 25 nM release complexes were then reacted with 62.5 nM ArfA and RF2 with concentrations of 50 nM – 30 μM at 37 °C for 1 sec to 30 min. The reactions were stopped by adding 5% ice cold trichloroacetic acid and spun at 18,000g for 10 min at 4 °C. The supernatant with released f-[^{35}S]-Met was counted using ScintiSafe Econo 1 Cocktail (Fisher Scientific). The maximally releasable fMet ($fMet_{Max}$) was measured by incubating 25 nM release complex with 100 μM

puromycin (Sigma-Aldrich) at 37 °C for 30 sec. The background level of released fMet in the absence of RF2 was measured at the same time points. The fraction of released fMet (the ratio between the released f-[^{35}S]-Met and fMet $_{Max}$) versus time was plotted and fitted to $F_t = F_{max} \cdot (1 - e^{-k_{obs} \cdot t})$. The k_{cat} and $K_{1/2}$ were obtained by plotting k_{obs} versus concentration of RF2 and fitting with $k_{obs} = k_{cat} \cdot [RF2]/(K_{1/2} + [RF2])$.

Formation of heterologous release complexes comprised of *E. coli* ribosome and *Thermus thermophilus* RF2

Thermus thermophilus (*T. thermophilus*) RF2 was co-expressed with its cognate methyltransferase in *E. coli* BL21 (DE3) strain [35] to achieve a full methylation of the GGQ motif and the resulting protein was purified as described previously [4]. To form the heterogolous nonstop ribosomal complexes, 50 μL of *E. coli* 70S ribosome (4 μM), mRNA (8 μM), tRNA^{fMet}, *E. coli* ArfA and *T. thermophilus* RF2 (16 μM each) were incubated at 37 °C for 30 min. The unbound factors were removed by size-exclusion chromatography using a Superdex 200 (10/30) column (Amersham/GE Healthcare). The ribosomal complex peak was collected and the binding of *T. thermophilus* RF2 to the *E. coli* ribosome was confirmed by SDS-PAGE.

Electron microscopy and image processing

Ribosomal complexes were formed by incubating ribosomes with mRNA, tRNA^{fMet}, ArfA and RF2 together at 37°C in a buffer containing 20 mM Hepes-KOH, pH 7.5, 15 mM magnesium acetate, 150 mM potassium acetate, 4 mM β-mercapthoethanol, 2 mM spermidine, 0.05 mM spermin [36].

Sample preparation for cryoEM was done using methods described [3738]. Aliquots of 2 μl nonstop ribosomal complex were incubated for 30 s on glow-discharged holey carbon grids with thin-layer carbon film (C-Flat TM Holey Carbon Grid CF-2/0.5–4C, 400 mesh, Copper, Protochips). Grids were blotted for 3.5 s in 100% humidity at 4°C and plunge frozen with a Vitrobot Mark IV (FEI). Data was collected in vitreous ice using a JEOL 3200 FS transmission electron microscope operating at 300 keV. A total number of 3,482 micrographs were acquired with a K2 summit direct electron detector (Gatan) operating in super mode at a calibrated magnification of 83,822 × (0.5965 Å per pixel) using a defocus range of −0.7 to −3 μm and a dose of 20 e^- per Å^2. Each micrograph was acquired as 30-frame movies during a 6s exposure. Movie frames were aligned using MotionCor2 to correct beam-induced motion and drift [39], and the aligned images were summed for further image processing. The Contrast Transfer Function (CTF) was estimated using CTFFIND4 [40]. All subsequent processing steps were performed in Relion [41-43]. Ribosome particles were picked using a semi-automated particle picking procedure [44], after which micrographs were inspected individually. Micrographs with improper defocus, ice contamination or poor CTF estimation were discarded. A total number of 445,164 particles were extracted from the 2,748 micrographs and were subjected to reference-free two-dimensional (2D) and 3D classifications in which non-ribosomal particles and particles for 50S, 30S were discarded. Statistical particle-based movie correction and radiation-damage weighing were performed [45] and the polished final 155,440 particles were subject to 3D refinement to yield a reconstruction at 3.52 Å.

Global, focused and local refinement

In global classification and refinement, a 3D classification of the 155,440 particles for the entire ribosome with a finer angular sampling of 1.8° and a local angular search range of 10° were performed, which led to two classes with different degrees of rotation of the 30S relative to the 50S subunit. The subsequent 3D refinement on these two classes yielded reconstructions of the nonstop complexes at 3.52 Å and 3.63 Å resolution, respectively (Extended Data Figs. 1c, 1d and 2a). Coupled with the global domain movements observed in the ribosome, the binding ligands including a nonstop mRNA, E-tRNA, ArfA and RF2 all show different degrees of displacement. Despite these differences, based on the reconstructions obtained from the two classes, binding of ArfA and RF2 in the ribosomal A site induces the same conformational changes in the decoding center of the ribosome. The 30S subunit adopts a “closed” conformation, and the CCA-end of the P-tRNA and the GGQ motif of RF2 are placed at the core of the PTC.

However, using the global classification and refinement procedure, the local resolution around the ArfA and RF2 region was estimated as 4–4.5 Å by ResMap [46] (Extended Data Fig. 2c). To obtain a higher resolution and a better resolved map of this region, we performed focused classification with or without signal subtraction [47-49] using masks over the ArfA and RF2 (Extended Data Figs 1c, 2d and 2f).

First, focused 3D classifications with a mask over ArfA and RF2 (ArfA/RF2), or a mask over ArfA, RF2 and 30S body domain (ArfA/RF2/30S body domain), were performed without orientational searches. This procedure led to one class from a total of 155,440 particles and a subsequent refinement of the particles in the class yielded reconstructions with an overall resolution at 4.5 Å and 3.7 Å, for mask over ArfA/RF2 and ArfA/RF2/30S body, respectively (Extended Data Figs. 1c, 2d and 2e). Second, local refinements with signal subtraction over regions around ArfA/RF2 and ArfA/RF2/30S body were performed, which led to reconstructions with an overall resolution at 3.7 Å for the mask applying over ArfA/RF2, and 3.6 Å for the one applying over ArfA/RF2/30S body domain (Extended Data Figs. 1c and 2f–2h).

The resolution was reported based on the gold-standard FSC=0.143 criterion, after applying a soft spherical mask on the two reconstructions refined from the half of the dataset independently [50]. Local resolution was estimated by using ResMap [46].

Model building

Maps obtained from local refinements were used first for building the structure of ArfA in the ribosome. Homology models generated by Phyre2 [51] and I-TASSER [52] were used as an intial guide, and regions of ArfA containing residue 8–14 and 24–37 were built *de novo* according to the EM map.

The ArfA structure thus built was fit as a rigid body into the overall map of the entire ribosomal nonstop complex. To build the ribosome structure, the high-resolution crystal structure of the *E. coli* ribosome (PDB: 4YBB) [53] was used and fit into the map using Chimera [54]. The body, head and shoulder domains of the 30S were fit separately. Subsequently, H69, H25, H43, H77, H84 of 23S rRNA, 5S rRNA, h44 of 16S rRNA and

most of ribosomal proteins were fit into the map individually. Homology model of *E. coli* RF2 was generated using SWISS-MODEL [55] from *T. thermophilus* RF2 (PDB: 4V5J) [26]. The switch loop of RF2 [25] was built according to the map obtained from the local refinement. Model building was done in COOT [56].

Model refinement and validation

The model was refined using Refmac5.8 [57] with secondary structure, RNA base-pair, sugar pucker and base stacking restraints generated by ProSMART [58] and LIBG [59]. The refinement weight was experimentally optimized in Refmac to balance the overall fit of the model to the map and the geometry of the structural model. Cross-validation of two half maps was done where Fourier shell correlation (FSC) was monitored. The final model was validated using MolProbity [60]. Extended Data Table 1 summarizes refinement statistics for the overall and local structures. Maps are visualized using Chimera and figures were generated using PyMOL [61] and Chimera.

Data Availability

EM maps have been deposited in the Electron Microscopy Data Bank under accession codes EMD-8505 for the entire nonstop complex and EMD-8506 for the map around ArfA region. Coordinates have been deposited in the Protein Data Bank under accession codes 5U4I for the entire ribosomal complex and 5U4J for the coordinate around the ArfA region.

Extended Data

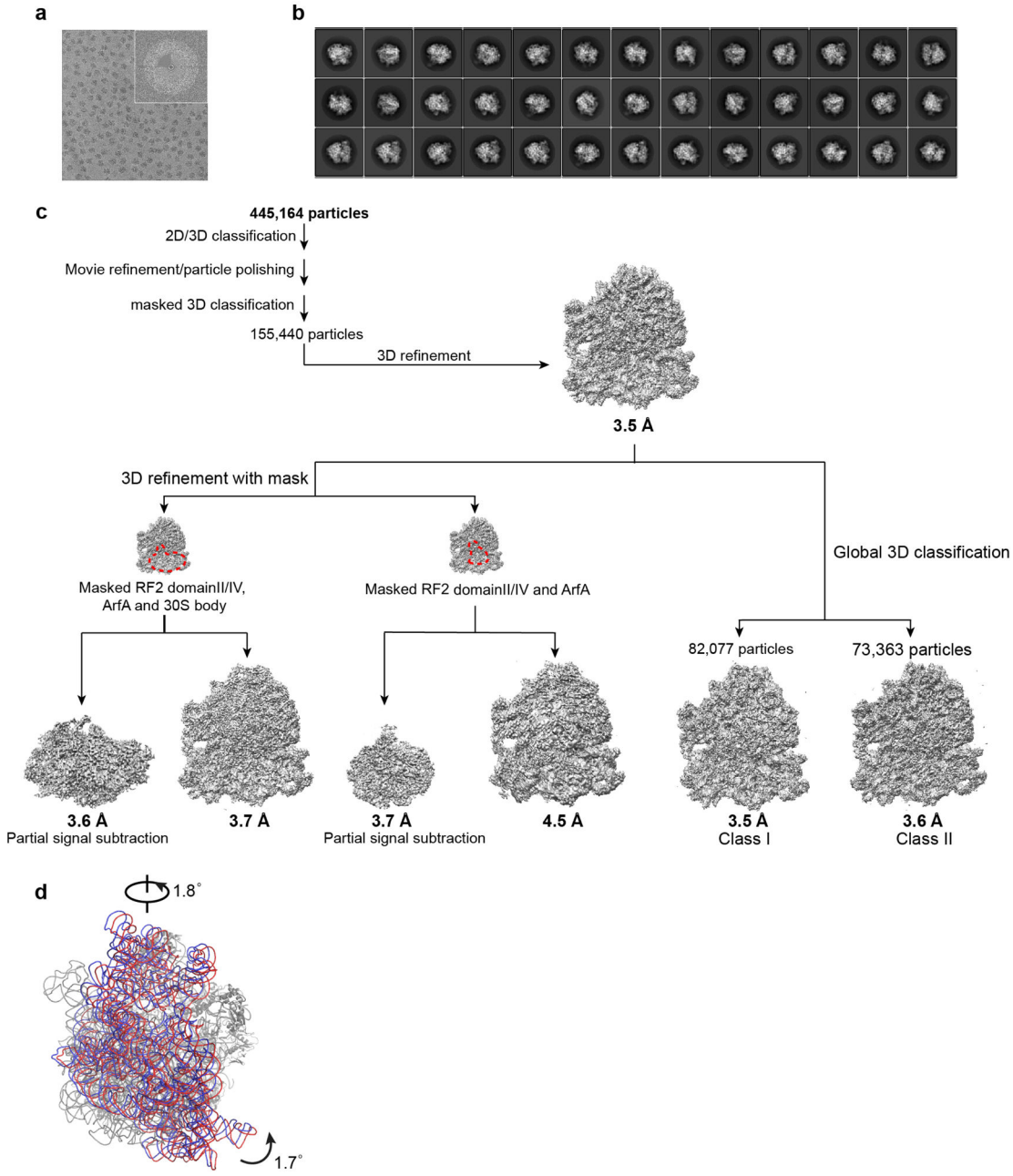

Extended Data Figure 1. Structure determination of 70S ribosome with ArfA and RF2 on a nonstop mRNA by cryoEM

a, A representative micrograph with corresponding FFT shown in an insert. The insert shows the CTF estimation of an average background-subtracted power spectrum and fitted CTF (top-left corner) using CTFFIND4 [40]. **b**, Representative 2D class averages from reference-free 2D classification. **c**, Particle classification and structural refinement procedures used to in this study. **d**, Conformational differences between the nonstop ribosomal complexes in the two classes obtained from the global classification and refinement. Rotation of the 16S

rRNA in the 30S subunit relative to the 23S rRNA in the 50S subunit from class I (red) to class II (blue) showing a 1.7° 16S body domain rotation and an orthogonal 1.8° head domain rotation. Ribosomes in the two classes were aligned using the 23S rRNA of the 50S subunit. Small subunit ribosomal proteins are not shown for clarity.

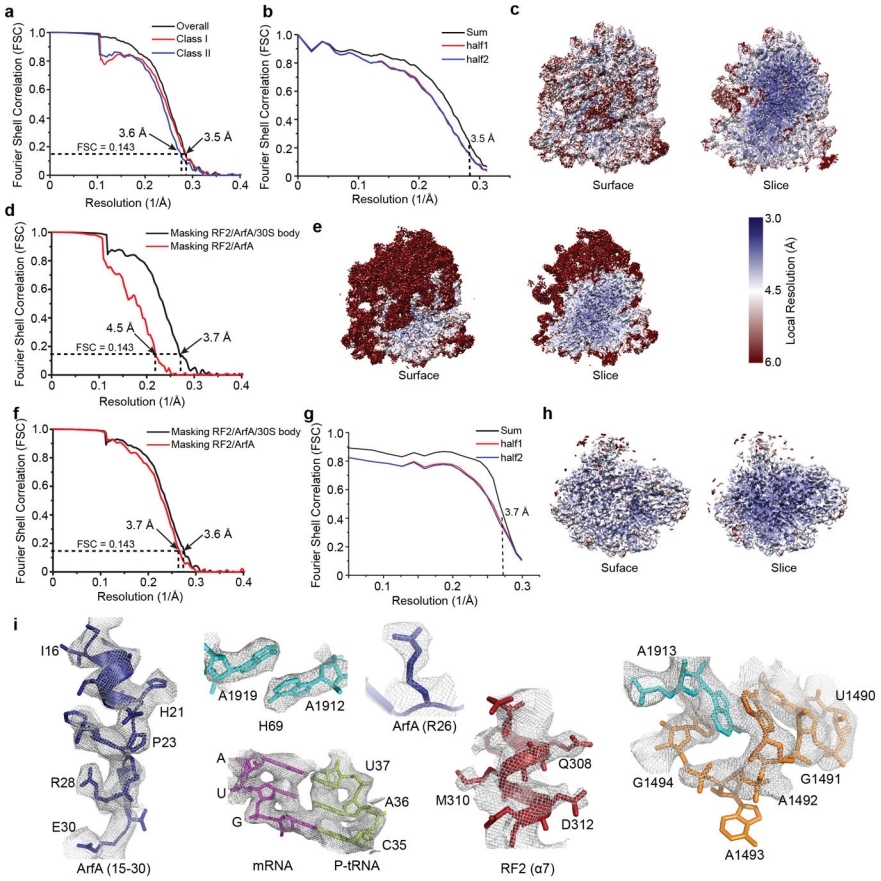

Extended Data Figure 2. Map and model quality

a, Gold standard FSC curves for the EM map from 155,440 particles (black), EM maps of class I (red, 82,077 particles) and class II (blue, 73,363 particles) from the global 3D classification and refinement. Resolution is demarcated using the FSC=0.143 criterion. **b,** Fit of the model to the map. FSC curves calculated between the refined structural model and the final EM map (sum, black), with the self-validated (half1, red) and cross-validated (half2, blue) correlations shown. **c,** The unfiltered and unsharpened density map colored by local resolution in surface and slide views for the entire nonstop ribosomal complex. **d,** Gold standard FSC curves for the EM maps obtained from the focused refinements with a mask over the ArfA/RF2/30S body domain (black) and a mask over the ArfA/RF2 region (red). **e,** Same as c for the EM map obtained from the focused refinement with a mask over the regions of ArfA, RF2 and the 30S body domain. **f,** Gold standard FSC curves for the EM maps obtained from the local refinement with partial signal subtraction using a mask over the ArfA/RF2/30S body domain (black) and a mask over the ArfA/RF2 region (red). **g,** Fit of the model to the map. FSC curves are calculated between the refined structural model and the final EM map (sum, black) for the ArfA and RF2 region, with the self-validated (half1,

red) and cross-validated (half2, blue) correlations shown. **h,** Same as c for the EM map obtained from the local refinement with a mask over the region of ArfA and RF2. **i,** Representative EM maps showing the refined structures of ArfA (density) and RF2 (firebrick), 23S rRNA (cyan) and 16S rRNA (orange).

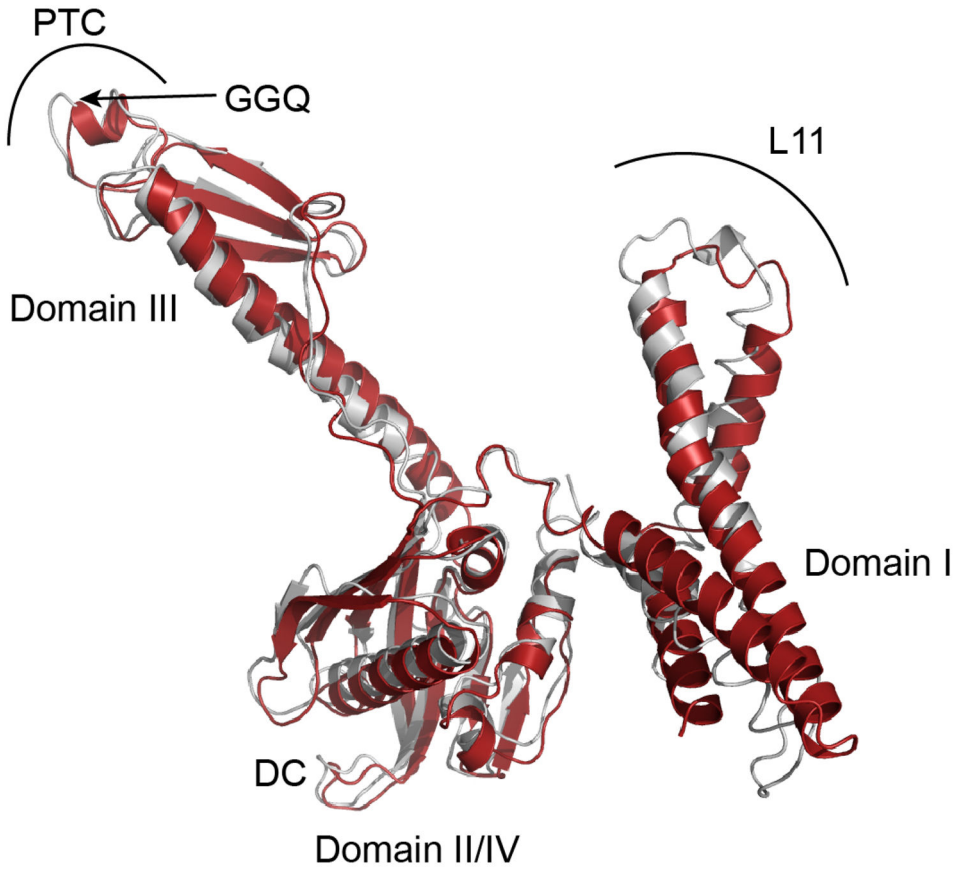

Extended Data Figure 3. Conformations of RF2 in the canonical and nonstop termination complexes

Superposition of structures of RF2 in the canonical termination complex from *Thermus thermophilus* (PDB code: 4V5J [26], colored in grey) and nonstop translation complex from *E. coli* (this study, colored in red) based on an alignment of the 16S rRNAs of the two ribosomal complexes. In both structures, domains II and IV of RF2 bind to the decoding center of the ribosome, domain III extends into the 50S subunit positioning the universally conserved GGQ motif into the peptidyl-transferase center, and domain I interacts with the L11 stalk and the 30S shoulder region.

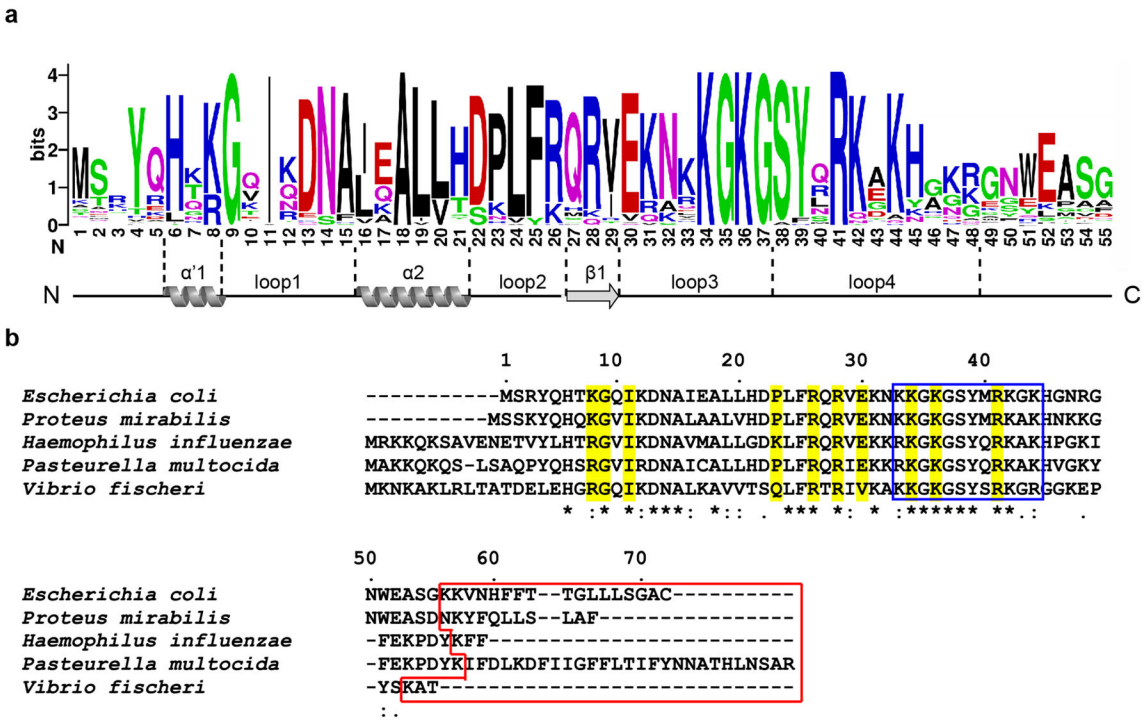

Extended Data Figure 4. Sequence alignment of ArfA from different bacterial species

a, Pictorial representation of the consensus sequence showing the frequency of different amino acids in residues 1–55 of ArfA from 66 species. Alignment was generated by Weblogo (http://weblogo.berkeley.edu/logo.cgi), where the amino acids are colored according to their chemical properties. Polar and uncharged amino acids (G, S, T, Y, C) are colored green, amino acids (Q, N) in purple, basic amino acids (K, R, H) in blue, acidic amino acids (D, E) in red, and hydrophobic amino acids (A, V, L, I, P, W, F, M) in black. Secondary structure features of ArfA from *E. coli* when it binds to the ribosome are shown according to the atomic structure obtained in this study. **b,** Multiple sequence alignment of ArfA proteins from different bacterial species showing that all ArfA proteins contain a positively charged C-terminal domain, as framed in the blue box. *E. coli* ArfA (NCBI GenInfo Identifier (GI) number 1450289), *Proteus mirabilis* ArfA (GI6802815), *Haemophilus influenza* ArfA (GI951152), *Pasteurella multocida* ArfA (GI29389120), and *Vibrio fischeri* ArfA (GI3280674) are used as examples. The red box indicates the C-terminal truncated region during ArfA maturation [17]. ArfA mutants used in this study are highlighted in yellow. Multiple sequence alignment was carried out in Clustal Omega [62].

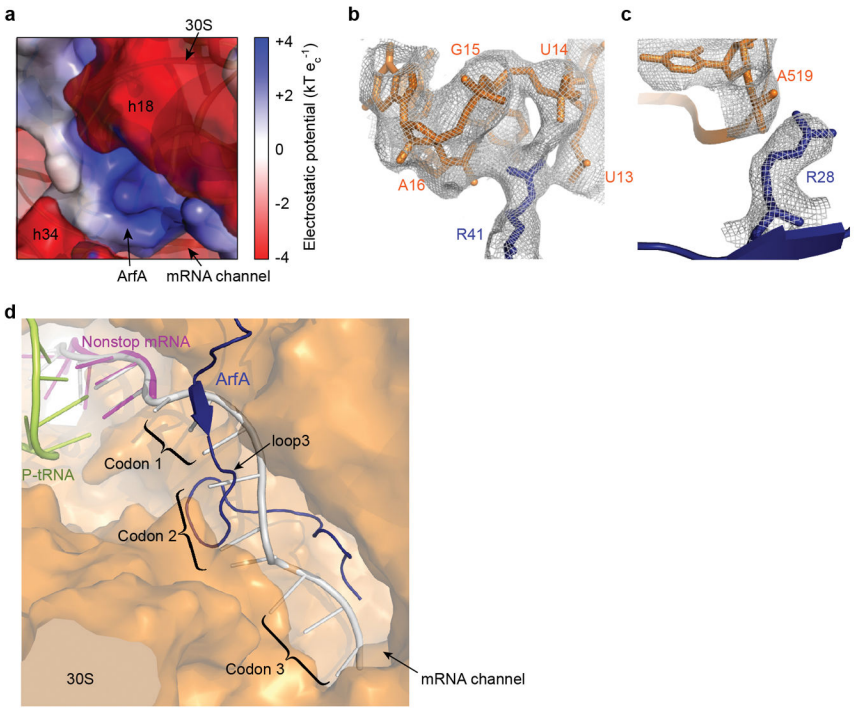

Extended Data Figure 5. Interactions of the C-terminal tail of ArfA with the ribosome

a, View of the mRNA entry channel showing the positively charged residues in the C-terminal domain of ArfA interacting with negatively charged phosphate backbones of rRNA. RF2 is omitted for clarity. Electrostatic potentials were calculated using APBS [63] with pdb2pqr [64], where k is Boltzmann's constant, T is the system temperature of the calculation (310K) and e_c is the charge of an electron. **b** and **c,** Positively charged residues in ArfA interact with phosphate backbones of the rRNA in the ribosome. Densities for selected ArfA residues are shown. R41 of ArfA makes contact with nucleotides in the mRNA entry channel in **b**. R28 of ArfA interacts with A519 of 16S rRNA in **c**. ArfA and16S rRNA are colored blue and orange respectively. **d,** Flexibility of the loop 3 (E30-G37) in ArfA allows for accommodation of a few nucleotides downstream the P-site in the ribosome. One to two codons downstream of the ribosomal P site appear to be accommodated by ArfA, and three codons downstream the P-site nearly abolishes the peptide release activity in the ribosome, consistent with the biochemical data [1,4,13]. The 30S is shown in yellow. ArfA, nonstop mRNA and P-tRNA are colored in blue, magenta and lemon, respectively. An mRNA (grey) taken from PDB 4V6F [65] was used in the figure for the purpose of illustration.

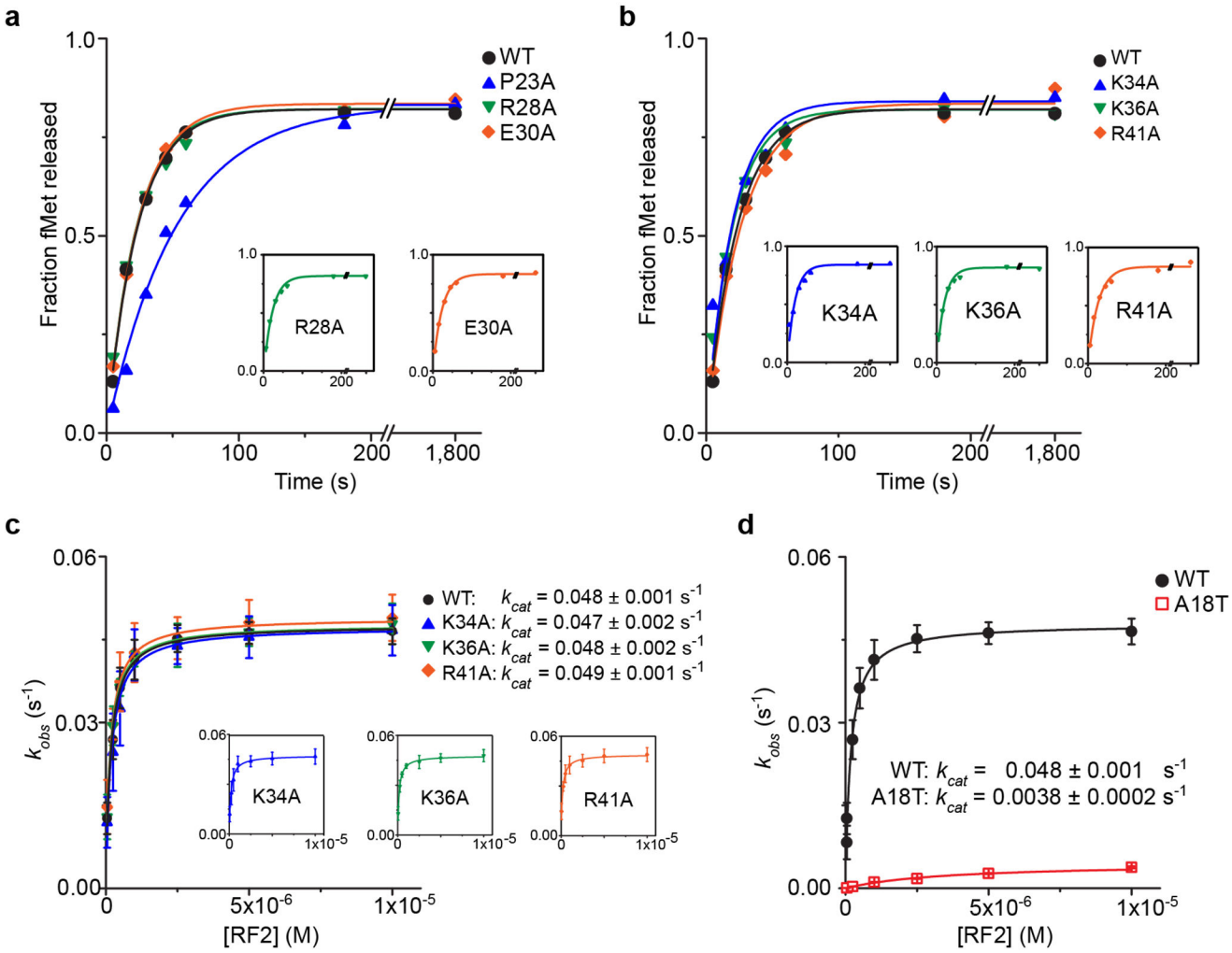

Extended Data Figure 6. Peptide release by RF2 and ArfA mutants in the nonstop stalled ribosome

a. Representative time courses of peptide release for ArfA mutants with point mutations on residues interacting with the ribosomal decoding center including P23A (▲), R28A (▼) and E30A (◆). **b.** Representative time courses of peptide release for ArfA mutants with point mutations in the C-terminal tail including K34A (▲), K36A (▼) and R41A (◆). Data on WT ArfA (●) are shown. Ribosomal complexes (25 nM) with nonstop mRNA and P-site fMet-tRNA^{fMet} were incubated with 62.5 nM ArfA and 5 μM RF2 at 37°C and the released peptides were measured at different time points after adding ArfA and RF2. **c.** Observed rate versus RF2 concentrations showing fits for catalytic rate constant k_{cat} and $K_{1/2}$ calculations for wild-type ArfA (●) and K34A (▲), K36A (▼) and R41A (♦) mutants. **d**, Observed rate versus RF2 concentrations showing fits for catalytic rate constant k_{cat} and $K_{1/2}$ calculations for WT ArfA (●) and A18T mutant (□). The k_{cat} and $K_{1/2}$ values on A18T, k_{cat} = 0.0038 ± 0.0002 s^{-1} and $K_{1/2}$ = 1.14 ± 0.28x10^{-6} M, were reported but the fitting curve was not shown [4]. The observed rate (k_{obs}) was determined as described in Methods. Catalytic rate constants and values of $K_{1/2}$ were obtained by fitting the observed rates versus the corresponding RF2 concentrations to Michaelis-Menten equation. An average of three

independent measurements is reported for each reaction and errors are calculated by standard error propagation.

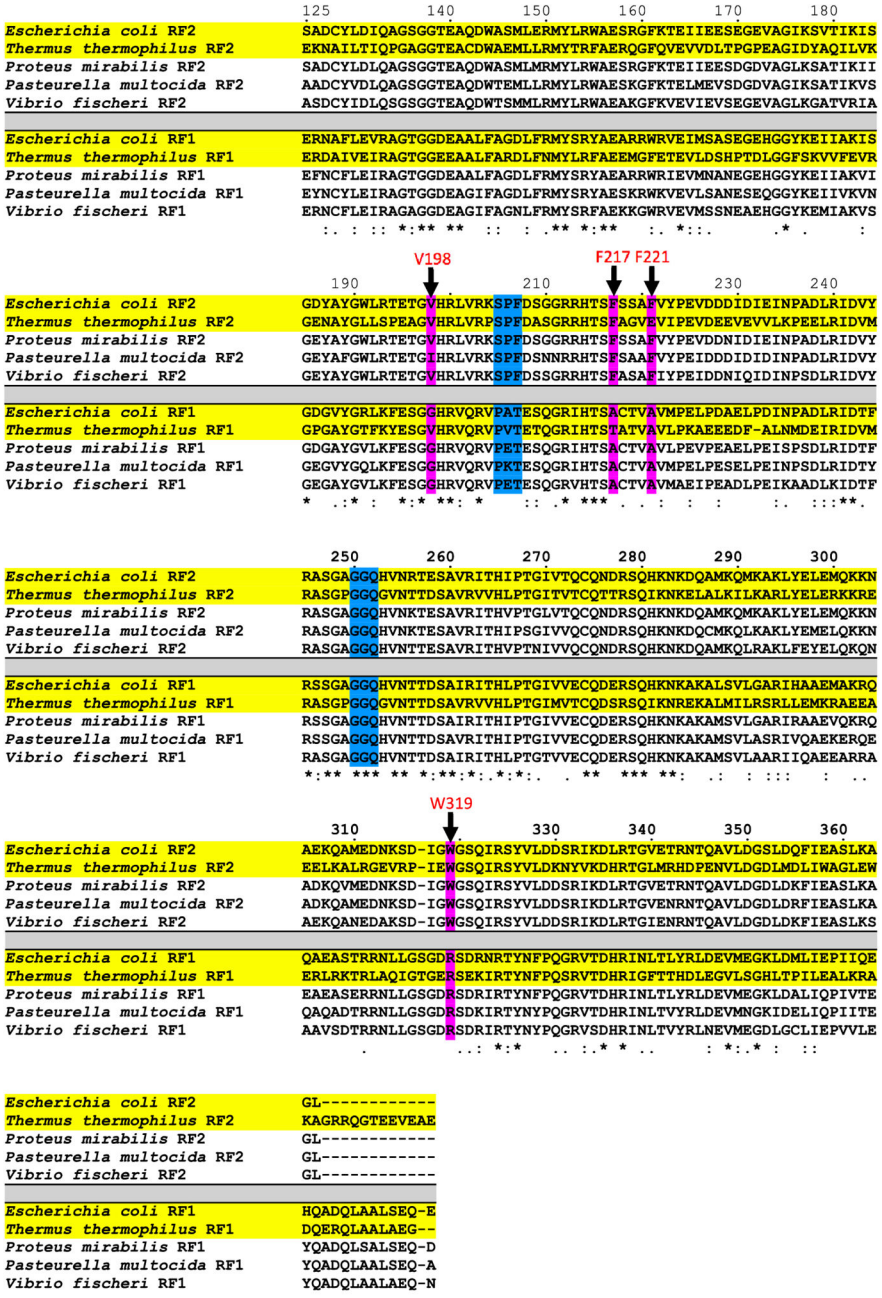

Extended Data Figure 7. Multiple Sequence alignment of the domain II-IV of RF2 and RF1 from different bacterial species

The *E. coli* RF1 (NCBI GenInfo Identifier number 949002) and RF2 (GI947369), *T. thermophilus* RF1 (GI3169506) and RF2 (GI3168831), *Proteus mirabilis* RF1 (GI6801441) and RF2 (GI23391224), *Pasteurella multocida* RF1 (GI29388454) and RF2 (GI29389590), *Vibrio fischeri* RF1 (GI3277422) and RF2 (GI3277319) were submitted to Clustal Omega for alignment. Except for the genome of *T. thermophilus* which does not contain a gene for

ArfA, genomes of other species all contain the ArfA gene [17]. The sequence alignment is validated by structural alignment of RF1 and RF2 [22,25]. Domain I of RF1 and RF2 are omitted for clarity. The SPF and GGQ motifs are highlighted in cyan, and the four functionally important residues discussed in this study (V198, F217, F221 and W319) are highlighted in magenta. Sequences of RF1 and RF2 from *E. coli* and *Thermus thermophilus* are highlighted in yellow.

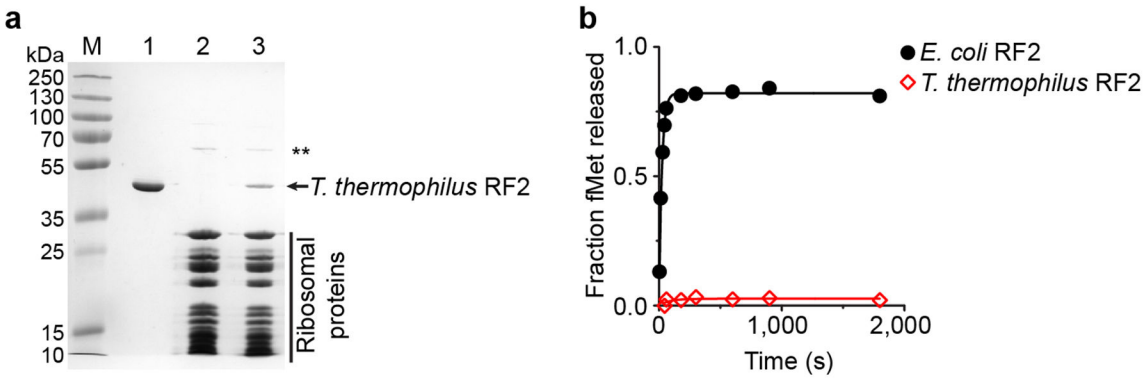

Extended Data Figure 8. A heterologous ribosomal nonstop complex can be formed *in vitro* but is biologically inactive

a, RF2 from *T. thermohpilus* binds to *E. coli* nonstop ribosomal complex *in vitro*. The heterologous nonstop ribosomal complex consists of RF2 from *T. thermohpilus* and ribosomes from *E. coli* was formed as described in Methods. SDS-polyacrylamide gel electrophoresis (SDS-PAGE) shows *T. thermophilus* RF2 (lane 1), apo ribosome from *E. coli* (lane 2) and the formation of heterologous nonstop ribosomal complex after gel filtration (lane 3). ** Denotes ribosomal protein S1. **b**, The heterologous ribosomal complex fails to catalyze peptide release. Representative time courses of peptide release by 5 μM of *E. coli* RF2 (●) and *T. thermophilus* RF2 (◊) at 25 nM nonstop stalled ribosome and 62.5nM ArfA from *E. coli* showing that *T. thermophilus* RF2 fails to catalyze peptide release in the ribosome.

Extended Data Table 1

Data collection and model statistics

	Local refinement	Global refinement
Data Collection		
Particles	445,164	
Pixel size (Å)	0.5965	
Defocus range (μm)	−0.7 to −3.0	
Voltage (kV)	300	
Electron dose (e^{-}Å^{-2})	20	
Model composition		
Non-hydrogen atoms	11,368	149,529
Protein residues	521	6,100

	Local refinement	Global refinement
RNA bases	494	4,715
Ligands (Zn^{2+}/Mg^{2+})	0/0	1/124
Refinement		
Resolution (Å)	3.7	3.5
Map sharpening B-factor ($Å^2$)	−50	−20
$FSC_{average}$	0.8424	0.7368
Rms deviations		
Bond lengths (Å)	0.0046	0.0051
Bond angles (°)	0.903	0.9606
Validation (proteins)		
Molprobity score	1.82 (100^{th})	2.61 (97^{th})
Clashscore, all atoms	2.86 (100^{th})	8.32 (97^{th})
Good rotamers (%)	97.18	91.96
Ramachandran plot		
Favored (%)	93.92	92.71
Outliers (%)	0.39	0.84
Validation (RNA)		
Correct sugar puckers (%)	96.46	98.68
Good backbone conformations (%)	78.31	70.24

Extended Data Table 2

Rate and binding constants of peptide release for wild-type and mutants of ArfA on the nonstop ribosomal complex

ArfA	Ribosomal complex	k_{cat} (s^{-1})	$K_{1/2}$ (10^{-6} M)
	WT	0.048 ± 0.001 *	0.16 ± 0.01 *
C-terminal region (Residue 33–44)	K34A	0.047 ± 0.002	0.18 ± 0.02
	K36A	0.048 ± 0.002	0.15 ± 0.01
	R41A	0.049 ± 0.001	0.15 ± 0.01
Central region (Residue 23–30)	P23A	0.026 ± 0.001	0.25 ± 0.03
	R26A	0.047 ± 0.001	0.16 ± 0.03
	R28A	0.048 ± 0.001	0.15 ± 0.03
	E30A	0.048 ± 0.001	0.14 ± 0.02
Activation domain (Residue 1–18)	Δ18N	0.0037 ± 0.0002	1.04 ± 0.15
	K8A	0.013 ± 0.001	0.25 ± 0.07
	G9V	0.013 ± 0.001	0.26 ± 0.04
	I11N	0.0040 ± 0.0004	0.95 ± 0.21

* Catalytic rate constants and values of $K_{1/2}$ were obtained by fitting the observed rates versus the corresponding RF2 concentration to Michaelis-Menten equation. An average of three independent measurements is reported for each reaction and errors are calculated by standard error propagation.

Acknowledgments

We thank Dr. Jian Peng in the University of Illinois at Urbana-Champaign for scripting, Dr. Wen Jiang from Purdue University, Dr. Yuan He from Northwestern University and Dr. Jun Liu from John P. and Kathrine G. McGovern Medical School for helpful suggestions on EM data collection and image processing, and members in the Jin lab for helpful discussions. The Gatan K2 direct electron detector was purchased with funds provided by the Chicago Biomedical Consortium and Searle Funds at The Chicago Community Trust. H.J. acknowledge the support from the National Institute of General Medical Sciences of the NIH (R01-GM120552 to H.J.). The computational part of the study was supported by the National Institute of General Medical Sciences (P41-GM104601 to J.C.P. and E.T.)

References

1. Shimizu Y. ArfA recruits RF2 into stalled ribosomes. J Mol Biol. 2012; 423:624–631. [PubMed: 22922063]
2. Chadani Y, Ito K, Kutsukake K, Abo T. ArfA recruits release factor 2 to rescue stalled ribosomes by peptidyl-tRNA hydrolysis in Escherichia coli. Mol Microbiol. 2012; 86:37–50. [PubMed: 22857598]
3. Chadani Y, et al. Ribosome rescue by Escherichia coli ArfA (YhdL) in the absence of trans-translation system. Mol Microbiol. 2010; 78:796–808. [PubMed: 21062370]
4. Zeng F, Jin H. Peptide release promoted by methylated RF2 and ArfA in nonstop translation is achieved by an induced-fit mechanism. RNA. 2016; 22:49–60. [PubMed: 26554029]
5. Rodnina MV. Quality control of mRNA decoding on the bacterial ribosome. Adv Protein Chem Struct Biol. 2012; 86:95–128. [PubMed: 22243582]
6. Keiler KC. Mechanisms of ribosome rescue in bacteria. Nat Rev Microbiol. 2015; 13:285–297. [PubMed: 25874843]
7. Giudice E, Gillet R. The task force that rescues stalled ribosomes in bacteria. Trends Biochem Sci. 2013; 38:403–411. [PubMed: 23820510]
8. Ito K, Uno M, Nakamura Y. A tripeptide ‘anticodon’ deciphers stop codons in messenger RNA. Nature. 2000; 403:680–684. [PubMed: 10688208]
9. Zaher HS, Green R. Quality control by the ribosome following peptide bond formation. Nature. 2009; 457
10. Frolova LY, et al. Mutations in the highly conserved GGQ motif of class 1 polypeptide release factors abolish ability of human eRF1 to trigger peptidyl-tRNA hydrolysis. RNA. 1999; 5:1014–1020. [PubMed: 10445876]
11. Mora L, et al. The essential role of the invariant GGQ motif in the function and stability in vivo of bacterial release factors RF1 and RF2. Molecular microbiology. 2003; 47:267–275. [PubMed: 12492870]
12. Dincbas-Renqvist V, et al. A post-translational modification in the GGQ motif of RF2 from Escherichia coli stimulates termination of translation. EMBO J. 2000; 19:6900–6907. [PubMed: 11118225]
13. Kurita D, Chadani Y, Muto A, Abo T, Himeno H. ArfA recognizes the lack of mRNA in the mRNA channel after RF2 binding for ribosome rescue. Nucleic Acids Res. 2014; 42:13339–13352. [PubMed: 25355516]
14. Rodnina MV, Beringer M, Wintermeyer W. Mechanism of peptide bond formation on the ribosome. Q Rev Biophys. 2006; 39:203–225. [PubMed: 16893477]
15. Youngman EM, He SL, Nikstad LJ, Green R. Stop codon recognition by release factors induces structural rearrangement of the ribosomal decoding center that is productive for peptide release. Mol Cell. 2007; 28:533–543. [PubMed: 18042450]
16. Garza-Sanchez F, Schaub RE, Janssen BD, Hayes CS. tmRNA regulates synthesis of the ArfA ribosome rescue factor. Mol Microbiol. 2011; 80:1204–1219. [PubMed: 21435036]
17. Schaub RE, Poole SJ, Garza-Sanchez F, Benbow S, Hayes CS. Proteobacterial ArfA peptides are synthesized from non-stop messenger RNAs. J Biol Chem. 2012; 287:29765–29775. [PubMed: 22791716]
18. Ogle JM, Murphy FV, Tarry MJ, Ramakrishnan V. Selection of tRNA by the ribosome requires a transition from an open to a closed form. Cell. 2002; 111:721–732. [PubMed: 12464183]

19. Klaholz BP, et al. Structure of the Escherichia coli ribosomal termination complex with release factor 2. Nature. 2003; 421:90–94. [PubMed: 12511961]
20. Korostelev A, et al. Crystal structure of a translation termination complex formed with release factor RF2. Proc Natl Acad Sci U S A. 2008; 105:19684–19689. [PubMed: 19064930]
21. Rawat UBS, et al. A cryo-electron microscopic study of ribosome-bound termination factor RF2. Nature. 2003; 421:87–90. [PubMed: 12511960]
22. Weixlbaumer A, et al. Insights into Translational Termination from the Structure of RF2 Bound to the Ribosome. Science. 2008; 322:953–956. [PubMed: 18988853]
23. Gagnon MG, Seetharaman SV, Bulkley D, Steitz TA. Structural basis for the rescue of stalled ribosomes: structure of YaeJ bound to the ribosome. Science. 2012; 335:1370–1372. [PubMed: 22422986]
24. Neubauer C, Gillet R, Kelley AC, Ramakrishnan V. Decoding in the absence of a codon by tmRNA and SmpB in the ribosome. Science. 2012; 335:1366–1369. [PubMed: 22422985]
25. Laurberg M, et al. Structural basis for translation termination on the 70S ribosome. Nature. 2008; 454:852–857. [PubMed: 18596689]
26. Jin H, Kelley AC, Loakes D, Ramakrishnan V. Structure of the 70S ribosome bound to release factor 2 and a substrate analog provides insights into catalysis of peptide release. Proc Natl Acad Sci U S A. 2010; 107:8593–8598. [PubMed: 20421507]
27. Schmeing TM, Huang KS, Strobel SA, Steitz TA. An induced-fit mechanism to promote peptide bond formation and exclude hydrolysis of peptidyl-tRNA. Nature. 2005; 438:520–524. [PubMed: 16306996]
28. Cammack KA, Wade HE. The sedimentation behaviour of ribonuclease-active and-inactive ribosomes from bacteria. Biochem Journal. 1965; 96:671. [PubMed: 5324303]
29. Bommer, U., et al. Ribosomes and polysomes. In: Graham, J., Rickwood, D., editors. Subcellular Fractionation: A Practical Approach. IRL Press; Washington, DC: 1997. p. 271-301.
30. Kurylo CM, et al. Genome sequence and analysis of Escherichia coli MRE600, a colicinogenic, nonmotile strain that lacks RNase I and the type I methyltransferase, EcoKI. Genome biology and evolution. 2016; 8:742–752. [PubMed: 26802429]
31. Wolfrum A, Brock S, Mac T, Grillenbeck N. Expression in E. coli and purification of Thermus thermophilus translation initiation factors IF1 and IF3. Protein Expr Purif. 2003; 29:15–23. [PubMed: 12729721]
32. Chadani Y, et al. trans-translation-mediated tight regulation of the expression of the alternative ribosome-rescue factor ArfA in Escherichia coli. Genes Genet Syst. 2011; 86:151–163. [PubMed: 21952205]
33. Schmitt E, et al. Crystallization and preliminary X ray analysis of Escherichia coli methionyl-tRNA fMet formyltransferase. Proteins: Structure, Function, and Bioinformatics. 1996; 25:139–141.
34. Walker SE, Fredrick K. Preparation and evaluation of acylated tRNAs. Methods. 2008; 44:81–86. [PubMed: 18241790]
35. Monteiro RA, Souza EM, Yates MG, Pedrosa FO, Chubatsu LS. Use of lactose to induce expression of soluble NifA protein domains of Herbaspirillum seropedicae in Escherichia coli. Canadian journal of microbiology. 2000; 46:1087–1090. [PubMed: 11109500]
36. Sprink T, et al. Structures of ribosome-bound initiation factor 2 reveal the mechanism of subunit association. Sci Adv. 2016; 2:e1501502. [PubMed: 26973877]
37. Stark H, Chari A. Sample preparation of biological macromolecular assemblies for the determination of high-resolution structures by cryo-electron microscopy. Microscopy. 2015:dfv367.
38. Grassucci RA, Taylor DJ, Frank J. Preparation of macromolecular complexes for cryo-electron microscopy. Nature protocols. 2007; 2:3239–3246. [PubMed: 18079724]
39. Li X, et al. Electron counting and beam-induced motion correction enable near-atomic-resolution single-particle cryo-EM. Nature methods. 2013; 10:584–590. [PubMed: 23644547]
40. Rohou A, Grigorieff N. CTFFIND4: Fast and accurate defocus estimation from electron micrographs. J Struct Biol. 2015; 192:216–221. [PubMed: 26278980]

41. Scheres SH. A Bayesian view on cryo-EM structure determination. J Mol Biol. 2012; 415:406–418. [PubMed: 22100448]
42. Scheres SH. RELION: implementation of a Bayesian approach to cryo-EM structure determination. J Struct Biol. 2012; 180:519–530. [PubMed: 23000701]
43. Kimanius D, Forsberg BO, Scheres SHW, Lindahl E. Accelerated cryo-EM structure determination with parallelisation using GPUs in RELION-2. eLife. 2016; 5:e18722. [PubMed: 27845625]
44. Scheres SH. Semi-automated selection of cryo-EM particles in RELION-1.3. J Struct Biol. 2015; 189:114–122. [PubMed: 25486611]
45. Scheres SHW. Beam-induced motion correction for sub-megadalton cryo-EM particles. eLife. 2014; 3:e03665. [PubMed: 25122622]
46. Kucukelbir A, Sigworth FJ, Tagare HD. Quantifying the local resolution of cryo-EM density maps. Nat Methods. 2014; 11:63–65. [PubMed: 24213166]
47. Bai X, Rajendra E, Yang G, Shi Y, Scheres SHW. Sampling the conformational space of the catalytic subunit of human -secretase. eLife. 2015; 4:e11182. [PubMed: 26623517]
48. Scheres SHW. Processing of Structurally Heterogeneous Cryo-EM Data in RELION. Methods in Enzymology. 2016
49. Nguyen THD, et al. Cryo-EM structure of the yeast U4/U6. U5 tri-snRNP at 3.7 Å resolution. Nature. 2016
50. Scheres SH, Chen S. Prevention of overfitting in cryo-EM structure determination. Nat Methods. 2012; 9:853–854. [PubMed: 22842542]
51. Kelley LA, Mezulis S, Yates CM, Wass MN, Sternberg MJE. The Phyre2 web portal for protein modeling, prediction and analysis. Nature protocols. 2015; 10:845–858. [PubMed: 25950237]
52. Zhang Y. I-TASSER server for protein 3D structure prediction. BMC bioinformatics. 2008; 9:1. [PubMed: 18173834]
53. Noeske J, et al. High-resolution structure of the Escherichia coli ribosome. Nat Struct Mol Biol. 2015; 22:336–341. [PubMed: 25775265]
54. Pettersen EF, et al. UCSF Chimera--a visualization system for exploratory research and analysis. J Comput Chem. 2004; 25:1605–1612. [PubMed: 15264254]
55. Biasini M, et al. SWISS-MODEL: modelling protein tertiary and quaternary structure using evolutionary information. Nucleic Acids Res. 2014; 42:W252–W258. [PubMed: 24782522]
56. Emsley P, Lohkamp B, Scott WG, Cowtan K. Features and development of Coot. Acta Crystallographica Section D: Biological Crystallography. 2010; 66:486–501. [PubMed: 20383002]
57. Murshudov GN, et al. REFMAC5 for the refinement of macromolecular crystal structures. Acta Crystallographica Section D: Biological Crystallography. 2011; 67:355–367. [PubMed: 21460454]
58. Nicholls RA, Fischer M, McNicholas S, Murshudov GN. Conformation-independent structural comparison of macromolecules with ProSMART. Acta Crystallographica Section D: Biological Crystallography. 2014; 70:2487–2499. [PubMed: 25195761]
59. Brown A, et al. Tools for macromolecular model building and refinement into electron cryo-microscopy reconstructions. Acta Crystallographica Section D: Biological Crystallography. 2015; 71:136–153. [PubMed: 25615868]
60. Chen VB, et al. MolProbity: all-atom structure validation for macromolecular crystallography. Acta Crystallographica Section D: Biological Crystallography. 2010; 66:12–21. [PubMed: 20057044]
61. Schrodinger, LLC. The PyMOL Molecular Graphics System, Version 1.7. 2015.
62. Sievers F, et al. Fast, scalable generation of high quality protein multiple sequence alignments using Clustal Omega. Molecular systems biology. 2011; 7:539. [PubMed: 21988835]
63. Baker NA, Sept D, Joseph S, Holst MJ, McCammon JA. Electrostatics of nanosystems: application to microtubules and the ribosome. Proceedings of the National Academy of Sciences. 2001; 98:10037–10041.
64. Dolinsky TJ, Nielsen JE, McCammon JA, Baker NA. PDB2PQR: an automated pipeline for the setup of Poisson-Boltzmann electrostatics calculations. Nucleic acids research. 2004; 32:W665–W667. [PubMed: 15215472]

65. Jenner LB, Demeshkina N, Yusupova G, Yusupov M. Structural aspects of messenger RNA reading frame maintenance by the ribosome. Nature structural & molecular biology. 2010; 17:555–560.

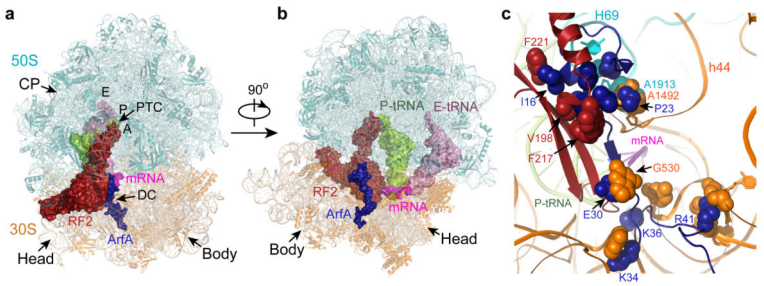

Figure 1. Structure of ArfA and RF2 bound to the ribosome on a nonstop mRNA

a. and **b.** Overall view of the ribosomal nonstop complex shows the structure of 70*S* ribosome in complex with $tRNA^{fMet}$ in the exit (E) and peptidyl (P) sites, a nonstop mRNA, and ArfA and RF2 in the A-site. ArfA (density), RF2 (firebrick), P-tRNA (lemon), E-tRNA (pink) and a nonstop mRNA (magenta) are shown in a surface representation. Ribosomal RNA and proteins are shown as cartoons. PTC, peptidyl transferase center; DC, decoding center; CP, central protuberance. **c.** An overview of ArfA in the ribosome viewing from the mRNA entry channel. Contacts between ArfA, RF2 with the ribosome are shown as spheres.

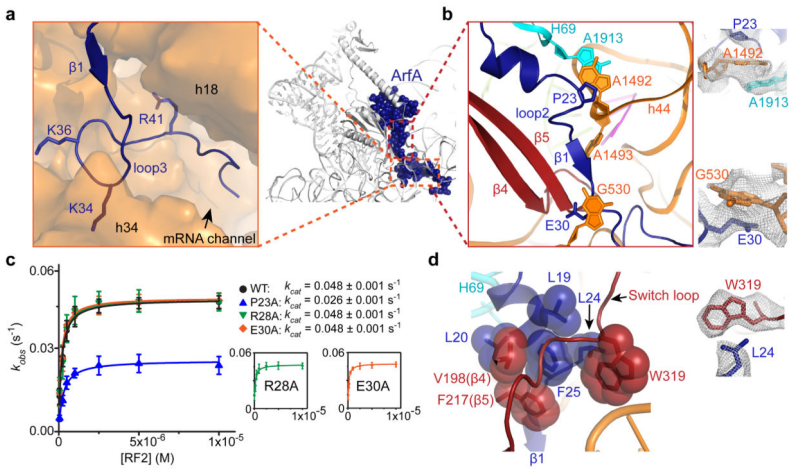

Figure 2. Interactions of ArfA and RF2 in the ribosome

a. The positively charged C-terminal tail of ArfA occupies the empty mRNA channel (surface, orange). **b.** Binding of ArfA and RF2 in the ribosomal A site. **c.** Observed rate versus RF2 concentrations showing fits for catalytic rate constant k_{cat} and $K_{1/2}$ for WT ArfA(●), and P23A (▲), R28A (▼) and E30A (♦) mutants. An average of three independent measurements is reported for each reaction and errors are calculated by standard error propagation. **d.** Hydrophobic interactions important for the recruitment of RF2 by ArfA in the ribosome. EM maps of important interactions are shown. ArfA (density), RF2 (firebrick), 16S rRNA (orange) and 23S rRNA (cyan).

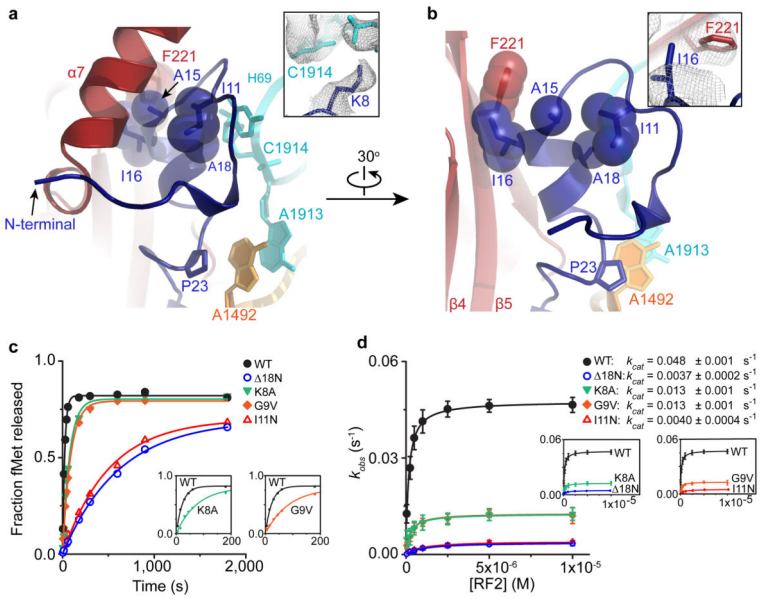

Figure 3. The activation domain of ArfA

a and **b.** The N-terminal domain of ArfA packs with α7 helix in RF2 and the B2a bridge formed between h44 and H69 in the ribosome. In **b**, α7 is removed to show the interaction between I16 in ArfA (density) and F221 in RF2 (firebrick). **c.** Representative time courses of peptide release at 25 nM nonstop ribosomal complexes by 5μM RF2 with 62.5 nM wild-type and mutant ArfA proteins. **d.** Observed rate versus RF2 concentrations showing fits for catalytic rate constant k_{cat} and $K_{1/2}$ calculations for wild-type ArfA (●) and mutant ArfA proteins. These mutants are: an N-terminal 18 amino acids truncated ArfA (Δ18N, ○), K8A (▼), G9V (♦) and I11N (▵). An average of three independent measurements is reported for each reaction and errors are calculated by standard error propagation.

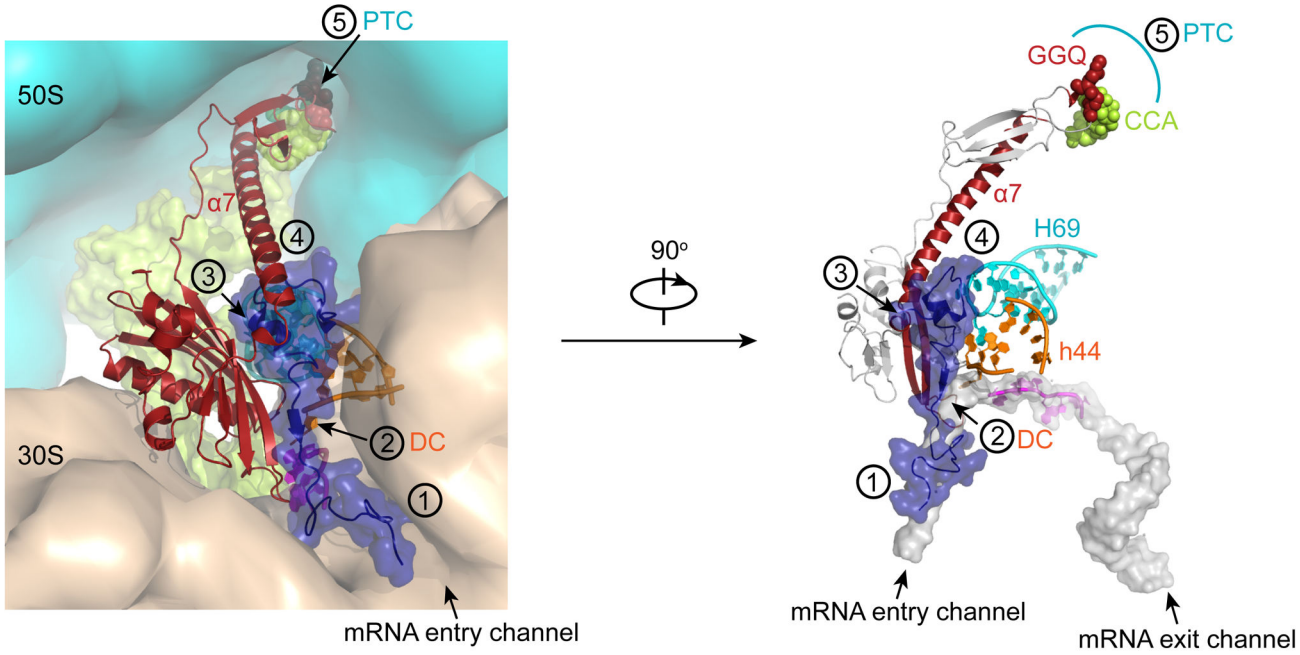

Figure 4. Schematic representation of sequential events involved in rescuing a nonstop translation by ArfA and RF2 in the ribosome

(1) Sensing and anchoring. The positively-charged C-terminal domain of ArfA senses an empty mRNA channel in the ribosome, where a highly conserved R41 and KGKG motif anchor the ArfA tail into the mRNA entry channel. (**2) Detecting an empty A site.** Relatively flexible loop regions in ArfA detect the presence of an empty ribosomal A site. (**3) Recruiting RF2 and accommodation.** Sequence-specific hydrophobic interactions in the N-terminal domain of ArfA recruit RF2. (**4) Activation.** The N-terminal helix and turn conformation mediated by hydrophobic interactions in ArfA and other interactions including I16 of ArfA and F221 of RF2 help induce RF2 into a catalytically competent conformation, docking the GGQ motif into the PTC in the large ribosomal subunit for (**5) Peptide release.**